Microfluidics and Nanofluidics (2023) 27:67
https://doi.org/10.1007/s10404-023-02678-9

RESEARCH

Effects of geometrical confinement on the generation of droplets at microfluidics T-junctions with rectangle channels

Kui He[1] · Zhiling Zhang[1] · Liangzhen Zhang[1] · Wuzhi Yuan[1] · Si-Min Huang[1]

Received: 12 July 2023 / Accepted: 26 August 2023 / Published online: 6 September 2023

Abstract

Despite the fact that there are not a few relative studies, the effects of geometrical confinement on droplets' generation at micro-T-junctions are not explicitly addressed. A three-dimensional volume of fluid (VOF) CFD model is developed here to study this classic microfluidics problem. The micro-T-junctions are designed with arms of a same hydraulic diameter but different width-to-depth ratios ($\chi = 1/10$–10), covering both deep-style ($\chi < 1$) and flat-style T-junctions ($\chi > 1$). It is found that the width-to-depth ratio (confinement style) shows complex effects on the dynamics of droplets' generation. At $\chi \leq 1/10$, droplets are failed to be generated at the T-junctions. Compared to the normal T-junctions ($\chi > 1$), the deep-style T-junctions ($1/6 < \chi < 1$) show much higher generation frequency of droplets at $\mathrm{Ca_c} > 0.06$ and the volume of generated droplets scales with $\mathrm{Ca_c}^{-1}$ instead of typical $\mathrm{Ca_c}^{-0.33}$. The comparative study of two paired T-junctions with reciprocal width-to-depth ratio (e.g., a deep-style T-junction, $\chi = 1/3$ and a flat-style T-junction, $\chi = 3$) explicitly illustrates that the geometrical confinement stabilizes the generation dynamics of droplets at T-junctions. The mechanism for the stabilization effect is discussed. It provides some new insights in terms of designing devices of droplets' generation.

Keywords Droplet flow · Micro-T-junction · Confinement effect · Comparative study

List of symbols

Ca	Capillary number, $\mathrm{Ca} = \mu_c U_c / \sigma$
D	Hydraulic diameter (m)
g	Gravity acceleration (m s^{-2})
H	Depth of a channel
m	Mass flow rate (kg s^{-1})
P	Gauge pressure (Pa)
U	Superficial flow velocity (m s^{-1})
W	Width of a channel

Greek letters

λ	Ratio of viscosity of oil and water
M	Dynamic viscosity (Pa s)
ρ	Density (kg m^{-3})
σ	Interfacial tension (N m^{-1})
τ	Shear stress (Pa)
χ	Ratio of width-to-depth of the channel

Subscripts

c	Continuous flow
in	Inlet of the T-junction
h	Hydraulic
s	Silicone oil
t	Total
w	Width, water, wall
x, y, z	Streamwise, normalwise, spanwise
1	Straight inlet of a T-junction
2	Side inlet of a T-junction
3	Outlet of a T-junction

1 Introduction

In recent years, droplet-based microfluidics appears in tremendous applications, such as biological analysis (Basova and Foret 2015), chemical reactors (Xu et al. 2008a), and nanomaterial synthesis (Xu et al. 2016). Sample encapsulation in the form of droplets avoids the sample dilution caused by Taylor dispersion (Bontoux et al. 2006) and increases mixing performance (Wang et al. 2014). The key process in those applications is how to generate uniform droplets with controlled volume. There are passive method and active method that can be used to generate droplets (Baroud

✉ Si-Min Huang
huangsm@dgut.edu.cn

[1] Guangdong Provincial Key Laboratory of Distributed Energy Systems, Guangdong Provincial Engineering Research Center of Distributed Energy Systems, Dongguan University of Technology, Dongguan 523808, China

et al. 2010). The former is more popular due to simplest process and low operation cost. In those passive devices, droplets are generated through various flow geometry, such as T-junctions (Garstecki et al. 2006; Xu et al. 2008b; Christopher et al. 2008; Gupta and Kumar 2010; Glawdel et al. 2012a; Bai et al. 2016), flow-focusing (Seo et al. 2007; Mulligan and Rothstein 2012; Hatch et al. 2013), and co-flowing geometries (Cramer et al. 2004; Utada et al. 2007; Hong and Wang 2007; Pan et al. 2021). In these devices, droplets are generated by shearing dispersed phase with a continuous stream of liquid. Among them, T-junctions are frequently used and studied due to its simplicity and better controlled droplet volume. The dispersed phase is trimmed periodically by the continuous flow at a junction. Volume and frequency of droplets can be adjusted by the flow rate ratio and the property of the two fluids. Numerous experiments are devoted to study the generation mechanism of droplets and establish the correlation for predicting the size of them (Liu and Zhang 2009; Glawdel et al. 2012a; Chen et al. 2011; Wehking et al. 2014). It is suggested that the droplet formation is governed by the interaction between shear stress and interfacial tension. The process of droplet formations in T-junctions is classified as three typical regimes, e.g., squeezing regime, dripping regime, and jetting regime. In the last 20 years, the critical condition for the transition between these regimes is an important topic (Thorsen et al. 2001; Garstecki et al. 2006; Christopher and Anna 2007; Gupta and Kumar 2010).

In the squeezing regime, the dominating contribution in the dynamics of droplet breakup arises from the buildup of pressure, which is resulted from the blocking of the cross section of the main channel by the body of dispersed phase. In this regime, it is found that the volume of droplets follows a simple correlation: $V = 1 + \alpha \frac{Q_d}{Q_c}$, where α is a constant of unity and it depends on the geometry of T-junctions. The volume of droplet size is almost independent of the fluids' properties. Sometimes, this generation mode is preferred because it allows changing the fluids while keeping the dynamics of formation similar. However, the generation rate at this regime is usually low and it is not desired for massive production of droplets. Comparably, in the regime of dripping and jetting regime, due to weakening of wall confinement, the correlation is strongly modified. The generation rate and the volume of the droplets exhibit a power law dependence on the capillary number for a fixed flow rate ratio (Husny and Cooper-White 2006; Xu et al. 2008b; De Menech et al. 2008). By identifying the inflection point at the correlation curves of droplets' volume against Ca_c, the critical value of Ca_c for the transition from squeezing to dripping is found between 0.01 and 0.02. De Menech et al. (2008) and Liu and Zhang (2009) respectively suggested two exact values 0.015 and 0.018 by analyzing numerical results. At a mediate Ca_c number, the range of Ca_c lying between 0.01 and 0.1, is suggested the dripping regime, where the size of droplets scales with Ca_c^{α} (Christopher et al. 2008; Xu et al. 2008b). The index α slightly varies from -0.33 to -0.2, which depends on the geometry design of the channel, ratio of viscosity of two fluids and wetting condition of the wall. At higher Ca_c number (>0.1), the reduction rate of volume of droplets becomes even higher and it scales with Ca_c^{-1} (Xu et al. 2006, 2008b). It is speculated that the change of scaling law is due to the size effect of the droplets. A corrected capillary number ($Ca\prime_c$) was put forward to build new correlations, which considers the size effect of droplets on the flow at the dripping regime ($0.01 < Ca_c < 0.1$). It is found that the size of droplets scales with ${Ca\prime_c}^{-1}$ at wide range of capillary numbers ($0.01 < Ca_c < 0.3$). A series of study shows that the generation process is almost not influenced by the ratios of viscosity of dispersed fluid and continuous fluid ($\lambda < 1$) and the flow rate ratios (Garstecki et al. 2006; Xu et al. 2008b; Christopher et al. 2008; Liu and Zhang 2009; Gupta and Kumar 2010; Glawdel et al. 2012a, 2012b; Chen et al. 2011; van Steijn et al. 2010).

The effect of geometry design on the generation of droplet is also an important topic, which indicates how the geometrical confinement affects the flow (Garstecki et al. 2006; van Steijn et al. 2010; Glawdel et al. 2012a, b; Wehking et al. 2014; Liu et al. 2015; Chakraborty et al. 2019; Paramanantham et al. 2022; Jena et al. 2023). Two typical changes of geometry have been regularly studied. In the first class, the depth of channels of T-junction is uniform and fixed, whereas the ratios of width of two inlets ($\Gamma = W_d/W_c$) varied (Garstecki et al. 2006; van Steijn et al. 2010; Glawdel et al. 2012a, b; Wehking et al. 2014). It is found that the increase of width of inlet of continuous fluid (W_c) results in bigger-sized droplets. Instead, designs with narrower inlet widths result in smaller droplets produced at higher rates. In the second class, the depth-to-width ratio of channels of T-junctions ($\chi = W/H$) is varied, whereas the ratio of width of two inlets is fixed. There are fewer cases for the latter class. By reducing the widths of channel but keeping the depth of the channel unchanged, it is found that the production frequency increases, but the size of droplets decreases as the χ reduces (van Stein et al. 2010; Liu et al. (2015); ; ; Paramanantham et al. 2022; Jena et al. 2023). It is speculated that the higher frequency and the lower size of droplets in a deeper T-junction are due to the faster filling stage in a channel of reduced widths. The droplet formation at squeezing regime is not entirely geometric. The size of droplets depends on both Γ and χ. Chakraborty et al. (2019) used quasi-2D depth-averaged Navier–Stokes equations to study the effects of χ, which was varied from 4.4 to 22. The results show that the droplet size decreases as $\sim {Ca_c}^{-1/3}$ at ultra-flat T-junction ($\chi > 8$), where the Ca_c working for this scaling law lasts from 0.002 to 0.06. The low limit of Ca_c is much lower than that observed at normal T-junctions, which is typically ~0.01 (Xu et al. 2008b). Generally, flatter T-junctions of high χ produce larger droplets in lower frequency. These observations are actually consistent to each other (van Steijin et al. 2010; Liu et al. 2015; Paramanantham et al. 2022; Jena et al. 2023). It is due to the fact that increasing the width of the channel is equivalent to the increasing of depth of the channel. It was not explained in details that why the critical value of Ca_c for the transition from squeezing to dripping was changed in ultra-flat T-junctions.

Previous study shows that variation of width-to-depth ratios is a way to understand the effects of geometrical confinement (Garstecki et al. 2006; van Steijn et al. 2010; Glawdel et al. 2012a, b; Wehking et al. 2014; Liu et al. 2015; Chakraborty et al. 2019; Paramanantham et al. 2022; Jena et al. 2023). But in those studies, confinement comes from at least three walls due to the flat-style design of the T-junctions. There is almost no relative study of T-junctions with width-to-depth ratios smaller than 1. This may be partly due to the fact that the deep-style T-junctions are not easy to be made by either soft lithography or machinery spinning. The T-junctions with small ratios of width-to-depth (e.g., $\chi=1/3$) are not reported so far and comparatively studied to those flat-style T-junctions (e.g., $\chi=3$). Although deep-style T-junctions are unusual, it is of scientific interest in at least two aspects. First, the two T-junctions ($\chi=1/3$ and $\chi=3$) form a special pair, whose channel is of rotational symmetry. As the capillary number and flow ratio are set at the same value in two paired T-junctions, the mean velocities (and thus the volume flow rate, Reynolds number and Weber number) of the flow at the two corresponding inlets are exactly the same. The velocity profiles at two inlets are rotationally symmetric about the axis of the channels. The symmetry is broken as the two fluids are approaching and contacting at the junctions. This setup is different to the previous relative study, in which there are always at least two parameters changed (volume flow rate and Reynolds number and area of cross section of channels). Second, 3-dimensional effects are important in the breakup process of a droplet. It is already shown that the breakup of a droplet is similar at filling stage for both 2D and 3D simulations but it is different at pinching-off stage (Hoang et al. 2013). In a 2D T-junction simulation, there is no confinement in depth direction. The depth is equivalent to infinite. Through systematically comparing the droplet generation at both super-flat and super-deep T-junctions (with strong and weak confinement in depth direction), it is to reveal how the 3D effects work during the generation of droplets and to find the critical width-to-depth ratio for the disappearance of 3D effects. It aims to provide some basic knowledge in terms of designing microfluidics T-junctions for generation of droplets. This paper employs a 3D VOF model to systemically examine the effects of width-to-depth ratios on the dynamics of droplets' generation at T-junctions. The χ is varied from 1/10 to 10, which forms 3 pairs of T-junctions with reciprocal width-to-depth ratios, covering both deep-style and flat-style T-junctions. The studied capillary number locates at a transitional regime (Ca = 0.004–0.08, Ca is the same to Ca_c hereafter).

2 Methodology

2.1 Numerical model

In this part, a 3D model is developed to investigate the generation dynamics of droplets at the junction part. Similar models have been used and validated to study the same class problem in several previous papers (Hoang et al. 2013; Soh et al. 2016; Nekouei and Vanapalli 2017; Sontti and Atta 2017). Following parts are the brief introduction of the model.

2.2 Governing equations

In present study, both dispersed and continuous phases are considered as Newtonian and incompressible fluids. The effect of gravity is ignored due to the micro-scale of the channel. The interface between the two fluids is tracked by the VOF method, where a single set of conservation equations for both phases is solved (Hirt and Nichols 1981).

Equation of continuity:

$$\frac{\partial \rho}{\partial t} + \nabla \times (\rho v) = 0 \tag{1}$$

Equation of momentum conservation:

$$\frac{\partial (\rho v)}{\partial t} + \nabla \times (\rho v v) = -\nabla P + \nabla \times \left[\mu\left(\nabla u + \nabla u^{\mathrm{T}}\right)\right] + S_{\alpha_q} \tag{2}$$

where P and S_{α_q} are pressure and surface tension force. The volume-averaged viscosity (μ) and the density (ρ) can be expressed in terms of continuous (α_{c}) and dispersed (α_{d}) phase volume fractions as:

$$\mu = \alpha_{\mathrm{c}}\mu_{\mathrm{c}} + (1-\alpha_{\mathrm{c}})\mu_{\mathrm{d}} \tag{3}$$

$$\rho = \alpha_{\mathrm{c}}\rho_{\mathrm{c}} + (1-\alpha_{\mathrm{c}})\rho_{\mathrm{d}} \tag{4}$$

Equation of volume fraction: The interface between the two liquid phases is traced by solving the following volume fraction continuity equation.

$$\frac{\partial \alpha_q}{\partial t} + v \times \nabla \alpha_q = 0 \quad (5)$$

where the subscript q refers to either continuous (c) or dispersed (d) phase. Furthermore, the volume fractions of both phases are conserved by $\sum \alpha_q = 1$. In case of $\alpha_q = 0$, the computational cell is assumed to be empty of the qth phase, and for $\alpha_q = 1$, the cell is considered to be completely filled with qth phase. Therefore, the fluid–fluid interface is estimated by identifying the cells with volume fraction range $0 < \alpha_q < 1$. To resolve the volumetric surface tension force (S_{α_q}) in Eq. (2), the continuum surface force (CSF) model (Brackbill et al. 1992) is applied here, as follows:

$$S_{\alpha_q} = \sigma \left[\frac{\rho \kappa_N \nabla \alpha_q}{\frac{1}{2}\left(\rho_c + \rho_d\right)} \right] \quad (6)$$

where κ_N is the interface curvature and σ is the coefficient of surface tension.

$$\kappa_N = \nabla \times \left(\frac{\nabla \alpha_q}{\left\| \nabla \alpha_q \right\|} \right) \quad (7)$$

In order to consider the effect of wall wetting, the normal of the interface is related to the wall's normal and tangential unit vectors,

$$n_{iterf} = \cos(\theta) n_{wall} + \sin(\theta) t_{wall} \quad (8)$$

where n_{iterf} is the normal of the interface. θ is the wall's static contact angle. n_{wall} and t_{wall} are the unit normal and unit tangential vectors to the wall, respectively.

2.3 Geometry and mesh setup

The dimensional parameters of the numerical T-junctions are listed in Table 1. The hydraulic diameter (D_h) of all the channels of T1 ~ T6 is roughly equal to 90 μm. The width-to-depth ratio χ varies from 1/10 to 10. The length of straight inlets (L_1) is equal to that of side inlets (L_2), which is equal to 10 D_h. The length of the outlet arms of these T-junctions (L_3) is about 20 D_h. The domain is longer enough to hold the longest droplets generated at the T-junctions for most cases. Effects of mesh resolution and mesh structure are studied first. Uniform hexagonal cells with different ratios of width-to-depth-to-length are generated. The length of cell in the flow direction is two times larger than in other two directions. The maximum distance of the first cell next to the wall is 3 μm. The similar mesh setup is also used in other papers (Soh et al. 2016; Rajesh and Buwa 2018). The test of mesh independence is shown in later section.

Table 1 Summary of geometrical parameters of the T-junctions (unit: μm)

Parameters	Channel depth (H)	Channel width (W)	Hydraulic diameter (D_h)
T1	50	500	91
T2	50	300	86
T3	60	180	90
T4	180	60	90
T5	300	50	86
T6	500	50	91

2.4 Boundary condition and numerical scheme

Water and silicone oil were selected as the working fluids. Water is the dispersed phase. The viscosity of water was fixed at 0.001 Pa s. The viscosity of oil was changed from 0.005 to 0.05 Pa s. The density of them is similar, which is about 980 kg m^{-3}. The interfacial tension between two phases is 0.029 N m^{-1}, which is a typical value measured for silicone oil in previous experiment (He et al. 2022). A constant velocity was applied at the inlet of both phases. The mean velocity of the continuous flow was varied between 0.0116 and 0.232 m s^{-1}. The ratios of mean velocity of continuous flow and dispersed flow were kept at a constant value (0.1, 0.25 or 0.5). The wettability of the wall has important effects on the topological of droplets (Wang et al. 2019). There are several ways in terms of treating the wettability of the wall. Most of the previous study considered it through a static contact angle. Table 2 summarizes the different treatments of contact angle (CA) used by these various CFD cases based on VOF method and level-set method. In these cases, the contact angles were set at different value. It varies from 0° to 180°. It is regretful that there is no rigorous reason for these treatments. The walls of the channels are considered as fully wetted by the continuous fluid (CA less than 5°). Practically, because there is always a thin oil film surrounding the water droplets, it needs very fine mesh to resolve it. Some researchers suggested that it is too expensive to resolve the super thin film (Chakraborty et al. 2019). Therefore, the contact angle was set as zero at the walls in this study. This treatment of contact angle guarantees that oil film doesn't dry out at the wall (Gupta et al. 2009). The solid walls were set to no-slip boundary condition. A constant atmospheric pressure boundary condition was set at the outlet of the T-junctions.

All the simulations were conducted in a finite volume CFD solver, Ansys Fluent 19. Pressure implicit with splitting operators (PISO) algorithm was used to calculate the pressure–velocity coupling in the momentum equation. Spatial derivative equations were discretized using a second-order upwind scheme, and the volume fraction was solved using Piecewise Linear Interface Construction (PLIC) algorithm.

Table 2 Summary of parameters of some relative papers

Paper	Contact angle (°)	Mesh resolution	Length of domain
Sontti and Atta (2017)	135	4 µm	50 W
Soh et al. (2016)	155	4 µm	34 W
Wang et al. (2019)	20–140	Unknown	12.5 W
Nekouei and Vanapalli (2017)	0	Unknown	Unknown
Chakraborty et al. (2019)	0	0.02 W	Unknown
Feigl et al. (2014)	180	2.5 µm	20 W
Hoang et al. (2013)	0	Unknown	11 W
Wehking et al. (2014)	180	2.0 µm	20 W

Variable time step and a fixed Courant number (Co = 0.25) were considered for simulating the governing equations. It is noteworthy that the implementation of the surface tension force can cause spurious currents across the interface in VOF modeling. To reduce such unphysical currents, Green–Gauss node-based gradient calculation was employed in this work.

3 Results and discussion

3.1 Validation of the model

The numerical method employed in this study has been validated in many previous studies (Hoang et al. 2013; Soh et al. 2016; Nekouei and Vanapalli 2017; Sontti and Atta 2017). It was reported that the VOF model predicted the generation of droplets well at a T-junction in terms of both quantitative and qualitative features, as long as a 3D simulation of high-quality mesh was conducted. In this paper, the model was validated by comparing the predicted scaling law with that drawn from experiments. The mesh independence test was carried out using T3 ($\chi = 3$). Capillary number, flow rate ratio, and viscosity ratio of water and oil are fixed at 0.01, 0.25, and 0.1, respectively. Figure 1 shows the variation of instantaneous volume flow rate of droplet ($\widetilde{V}_{\text{drop}}$) against time at three mesh setups, where the time sampling interval is 2×10^{-5} s. Figure 1a shows the structure of the mesh. In the model, each hexahedral cell is the same and the ratio of length of each cell in flow direction and two wall normal directions is 2: 1: 1 ($\Delta x_1 : \Delta x_2 : \Delta x_3$). The length of a cell in wall normal direction (Δx_2) is referred to characterize the mesh setups. Figure 1b shows that the profile of the instantaneous volume flow rate ($\widetilde{V}_{\text{drop}}$) converges together as the Δx_2 is reduced to 3 µm. Coarser mesh leads to lower generation frequency and larger droplet size. The maximum number of the hexahedral elements reaches about two million as the Δx_2 is equal to 3 µm.

In Fig. 2, the normalized mean volume of a droplet measured at the outlet of a typical flat-style T-junction ($\chi = 3$) is plotted against the capillary number of the continuous flow. The mean volume of droplets is calculated from following equations:

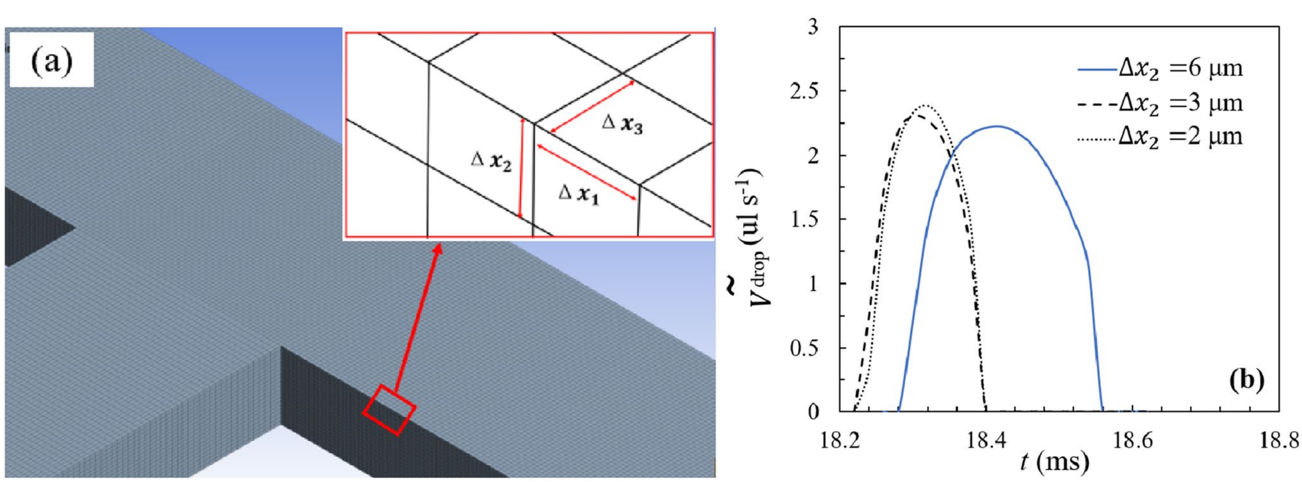

Fig. 1 The structure of the mesh (**a**) and independence test (**b**) of the mesh (T3, Ca = 0.01, $\varphi = 0.25$, $\lambda = 0.1$)

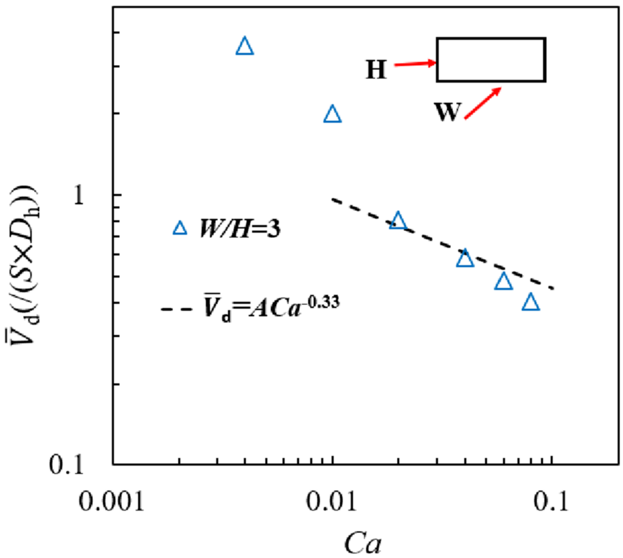

Fig. 2 Scaling law of the normalized mean volume of droplets at a typical flat T-junction (T3, $\varphi=0.25$, $\lambda=0.1$)

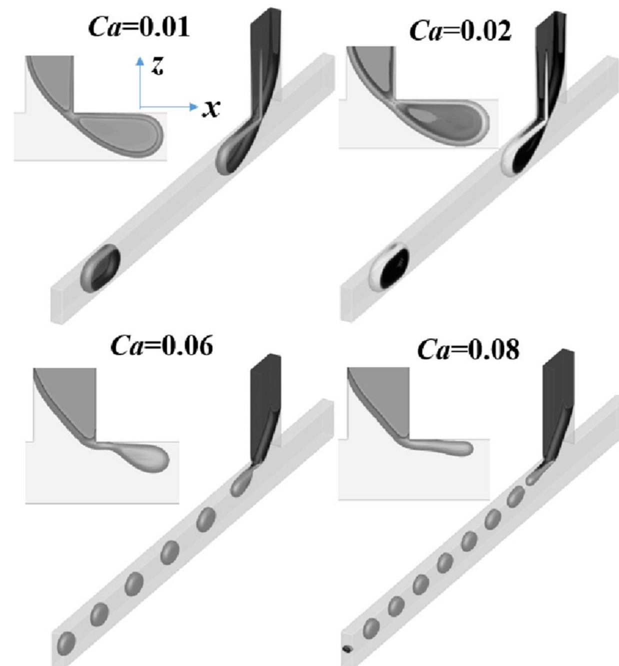

Fig. 3 Snapshots of droplet flow at different capillary numbers (T3, $\varphi=0.25$, $\lambda=0.1$)

$$\overline{V}_{\mathrm{d}} = \left(\int_{T_1}^{T_2} \widetilde{V}_{\mathrm{drop}} \mathrm{d}t\right)/N \tag{9}$$

where T_1 and T_2 are the start and end time of the sampling, respectively. During T_1 and T_2, N droplets pass the outlet of the T-junction. N is set at 20 for all cases. The mean volume is normalized by the cross-sectional aera of a channel (S) times the hydraulic diameter of the channel. Figure 2 shows that the normalized volume scales with the Ca in a power law, where the index of power is -0.33. The scaling law starts around 0.02 and ends around 0.08. It agrees with the correlations drawn from experiment and simulations (Xu et al. 2008b; De Menech et al. 2008).

Figure 3 shows several snapshots of droplet flow at different capillary numbers. At Ca = 0.01, the water droplet occupies the channel, leaving a thin film near the wall. It is a typical squeezing mode of droplet generation, in which pressure dominates the pinching-off of the droplets. At Ca = 0.02, the body of a water droplet becomes shorter and the gaps between the body and the wall are larger before the pinching-off. It is in a transitional regime. At Ca = 0.06, the size of the droplets is apparently smaller than the channel and they are formed near the junction. It usually refers to a dripping regime. At Ca = 0.08, the droplets are formed at the tongue of a water stream or a jet, which is a typical jetting regime. It is demonstrated that the numerical model predicts the generation of droplets well in terms of both quantitative and qualitative features.

3.2 General effects of width-to-depth ratio

Figure 4a shows the generation frequency of droplets at T-junctions with various ratios of width-to-depth ($\chi = W/H$). The χ varies between 1/10 and 10. The viscosity and the flow ratios of water and oil (λ and φ) are fixed at 0.1 and 0.25, respectively. At $\chi = 0.1$, there are no droplets generated at the studied domain, so it is not included in the figure. The reason for the failed droplet generation is discussed in Sect. 3.4. For other cases, it is shown that the generation frequency almost collapses together at Ca ranging from 0.004 to 0.06. Ratios of width-to-depth have almost no effects on the droplet' generation at these Capillary numbers. As the Ca is varied from 0.02 to 0.06, the generation frequency follows a power law in the form of $f \sim \mathrm{Ca}^{4/3}$. Correspondingly, Fig. 4b depicts that the volume of a droplet scales with $\mathrm{Ca}^{-0.33}$. The scaling law agrees with that drawn from previous experimental study (Xu et al. 2008b; Bai et al. 2016). It was reported that the volume of a droplet scales with $\mathrm{Ca}^{-\alpha}$. The power index lies between -0.4 and -0.3, as the Ca varies between 0.02 and 0.1. At the flow of larger capillary numbers ($0.06 < \mathrm{Ca} < 0.08$), the generation frequency increases much faster in these deep-style T-junctions. The volume of a droplet scales with Ca^{-1}. It shows that smaller χ leads to higher production rate of droplets and smaller volume of droplets at high capillary numbers. The mechanism for this observation is further discussed in Sect. 3.4.

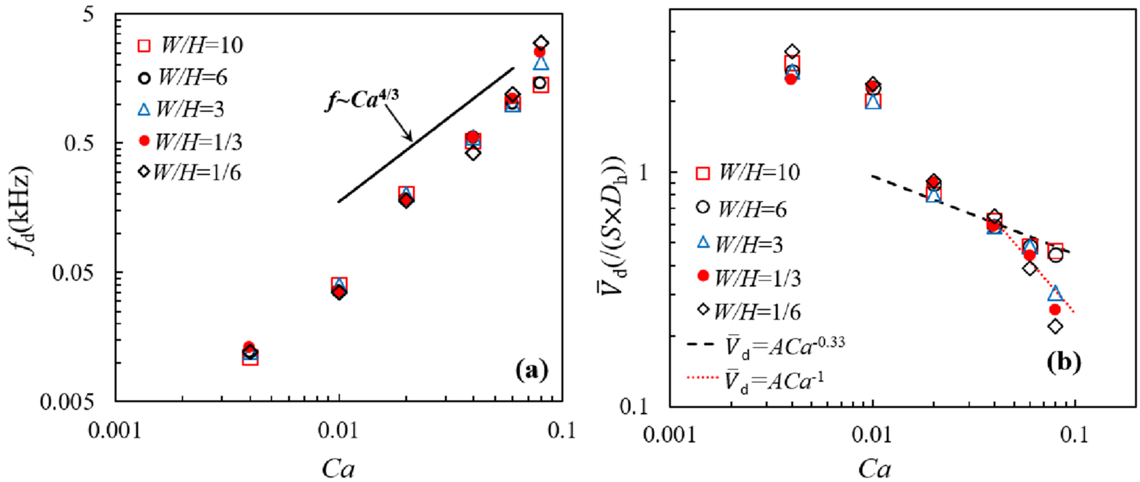

Fig. 4 The generation frequency (**a**) and non-dimensional size (**b**) of droplets at T-junctions with various ratios of width-to-depth

3.3 Effects of ratios of flow rates and viscosity of two fluids on a super-flat T-junction

As it is reviewed in the introduction, there are quite a lot of experiments and simulations related to the droplet generation at normal T-junctions, so this paper only focuses on the droplet generation at some special T-junctions, such as super-flat T-junctions ($\chi \geq 6$) and deep-style T-junctions ($\chi \leq 1/3$). Two unaddressed questions are interesting. The number one is that if the features of scaling law are only dependent on the Ca number of flows at the super-flat T-junction. This is examined by analyzing the effects of viscosity ratio of two fluids and velocity ratio of two flows. The number two is the mechanism that the scaling law of $f \sim \mathrm{Ca}^{-0.33}$ lasts for wider range of Ca numbers at super-flat T-junctions. The mechanism that the generation frequency becomes much higher at deep-style T-junctions is also interesting. In order to convince the results, it is also comparatively studied with the previous reports (Thorsen et al. 2001; Nisisako et al. 2002; Xu et al 2006; Garstecki et al. 2006; Glawdel et al. 2012a; Wehking et al. 2014; Nekouei and Vanapalli 2017; Loizou et al. 2018).

The data of T-junctions with $\chi = 10$ and $\chi = 1/3$ are selected and studied comprehensively. First, effects of ratios of flow rate and viscosity of fluids on the generation of droplets at a super-flat T-junction are discussed. In Fig. 5a, the generation frequency of droplets at various flow ratios of water and oil (φ) at T1 is plotted against the capillary numbers. The ratio of viscosity of water and oil is fixed at 0.1. As the φ varies from 0.1 to 0.4, it shows almost no effects on the generation frequency of droplets at Ca between 0.02 and 0.04. At $\varphi = 0.4$, the frequency is slightly higher at Ca between 0.004 and 0.02. As the flow rate of water is increased, the growth of droplet body is faster at the filling

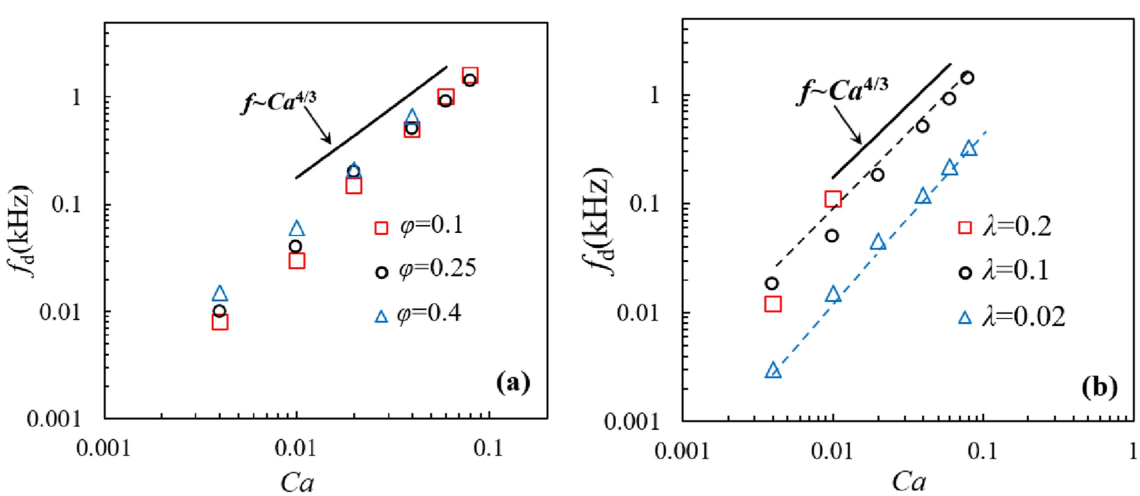

Fig. 5 Effects of flow rate ratios (**a**) and viscosity ratios (**b**) of water-to-oil on the generation frequency of droplets ($\lambda = 0.1$, $\chi = 10$)

stage of flow with $\varphi = 0.4$, which leads to slightly higher generation frequency. At $\varphi = 0.4$ and Ca > 0.06, the flow is stratified at the domain and no droplets are generated. The increase of flow ratio leads to more robust water jets (the width of them becomes larger) and they don't break up in the domain. Overall, the ratio of flow rates doesn't affect the generation frequency. The volume of the droplets linearly scales with the ratio of flow rates. The variation of the flow ratio leads to the change of the flow patterns, causing parallel flow at certain parameters. These observations are also consistent to previous experimental results (Wehking et al. 2014; Loizou et al. 2018), which showed that variation of flow rate ratios ($\varphi < 1$) results in almost linear variation of droplet' volume in normal T-junctions.

Comparing to the ratio of flow rates, the ratio of viscosity of water and oil (λ) shows more noticeable effects. In Fig. 5b, the ratio of flow rate of water and oil is fixed at 0.25. As the ratio of viscosity of water and oil is 0.2, the generation frequency of droplets is similar to these of lower λ value ($\lambda = 0.1$). No droplets are generated at the T-junction at capillary number larger than 0.02. The flow is stratified at the channel (not shown). As the viscosity of oil is increased to 50 times of the corresponding feature of water, the generation frequency becomes much lower than those with higher λ. But it still follows the power scaling law. The generation frequency was reduced to about 1/3 of the flow with $\lambda = 0.1$. The water flow rate at the inlet is reduced to 1/5 of the flow with $\lambda = 0.1$ as the capillary number is kept the same. It is straightforward to estimate that the mean volume of the droplets at $\lambda = 0.02$ is almost decreased by 40% (not plotted). Previous study also showed that more viscous continuous flow leads to decreased volume of the droplets (Thorsen et al. 2001; Nisisako et al. 2002; Xu et al 2006; Garstecki et al. 2006; Nekouei and Vanapalli 2017). Figure 6 show 2D snapshots of droplet flows ($\lambda = 0.1$ v.s. $\lambda = 0.02$) at a period of a droplet formation. It is seen that the droplets of high viscosity ratio are generated at just the junction but droplets of low viscosity ratio are generated at the tongue of a long jet. The former is a typical dripping flow but the latter is a jetting flow. As the capillary number of the two flows is the same, the change of velocity results in much higher variation of shear stress for the flow with $\lambda = 0.1$, which scales with U_c^2(Gupta et al. 2009). So the long jet in the flow with less viscous continuous fluid is induced by higher shear rate at the interface. Another interesting observation is the interface at the side arm, which is depressed to the water side. This topological structure is different to those observed in a normal T-junction (shown in Fig. 3). Usually, the interface is depressed to the oil side (Glawdel et al. 2012a; Nekouei and Vanapalli 2017). Due to the strong confinement in depth direction, the pressure at the inlet of a super-flat T-junction is much higher and it

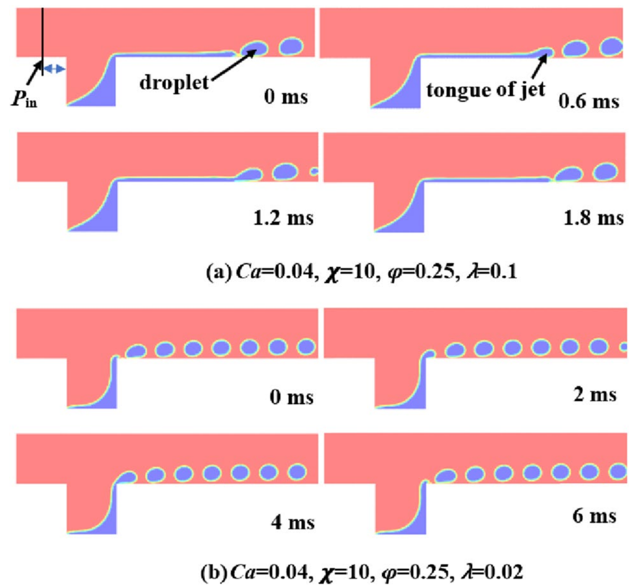

Fig. 6 Snapshots of several droplet flows of two viscosity ratios

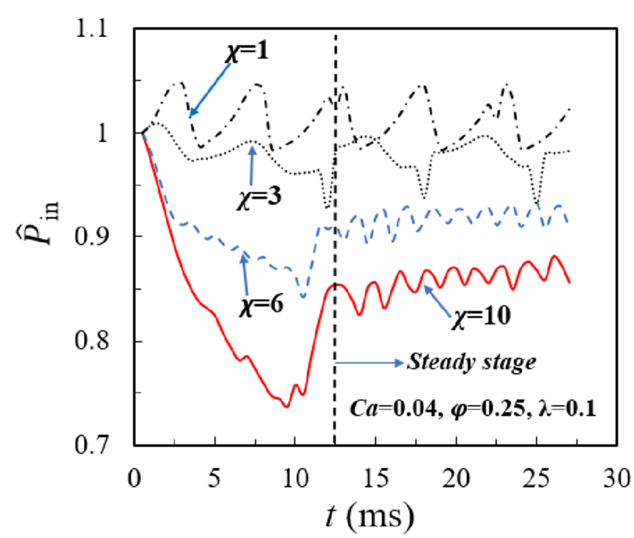

Fig. 7 Time variation of normalized pressure at the inlets of several T-junctions

overcomes the interfacial force. Figure 7 shows the time variation of the normalized pressure ($\hat{P}_{in} = \frac{P_{in,t}}{P_{in,t0}}$, where $P_{in,t0}$ is the initial referenced pressure at the inlet, 10 µm upstream to the edge of junction) of several droplet flows at different T-junctions. The sampling time interval is 0.5 ms. The flow takes more time to relax at the channels with χ higher than 6. At t < 12ms, the pressure reduces significantly at $\chi = 6$ and 10. It is due to the depression of interface into the side inlets. At the later stage, it shows that the $\hat{P}$ fluctuates with larger amplitudes at smaller χ and it becomes more and more gradual as the χ is increased. The fluctuations are induced by the blocking of droplets in the channel. It indicates that the influence of pressure becomes weaker in flatter T-junctions ($\chi \geq 6$).

3.4 Comparative study of droplets' generation at two paired T-junctions

It is interesting shown in Sect. 3.2 that the generation frequency of droplets is not influenced by the χ at low Ca numbers, but it becomes apparently higher at high *Ca* numbers in deep-style T-junctions ($\chi \leq 1/3$). Further increasing of χ to 1/10 results in failed generation of droplets at the T-junction. In this section, the droplet generation at two paired T-junctions are comparatively studied to reveal the mechanism for these detected differences. Figure 8 shows the time variations of normalized pressure at the inlets of two paired T-junctions at $Ca = 0.08$. The pressure is fetched at the inlet of oil (colored in red), 10 μm upstream at to the edge of junction. It is normalized by the inlet pressure at $t = 0$ ms. They are 17,976 Pa and 22,174 Pa for the deep-style and flat-style T-junctions, respectively. The sampling time interval is 0.02 ms. The peaks on the curves are marked and the corresponding snapshots of the droplets are depicted in Fig. 9. Figure 8 shows that the patterns of the time-variations of normalized inlet pressure at two T-junctions are similar in general but different in details as the capillary number is the same. The amplitudes of the fluctuations of the normalized inlet pressure at both cases are similar. It is about − 1 to − 1.5% of the averaged value at Ca = 0.08. At both T-junctions, the pressure increases at the stage I (1/1′ to 2/2′) from a trough. The pressure increases because a water droplet flows out of the domain and the water tongue grows at the tips (shown in Fig. 9). It slightly decreases at

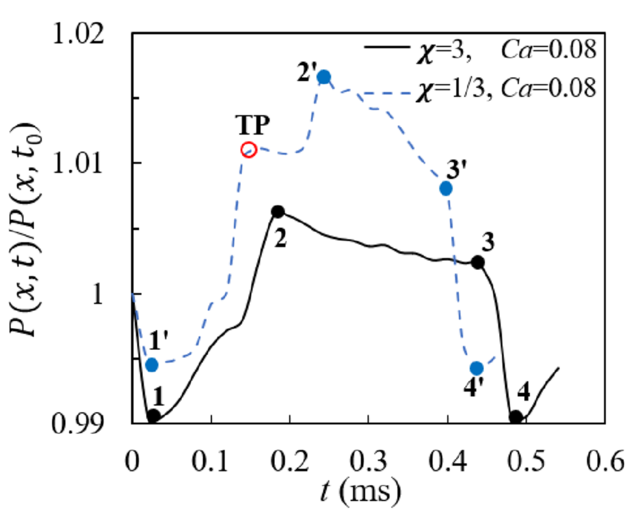

Fig. 8 Variations of normalized inlet pressure against time during a generation period of a droplet

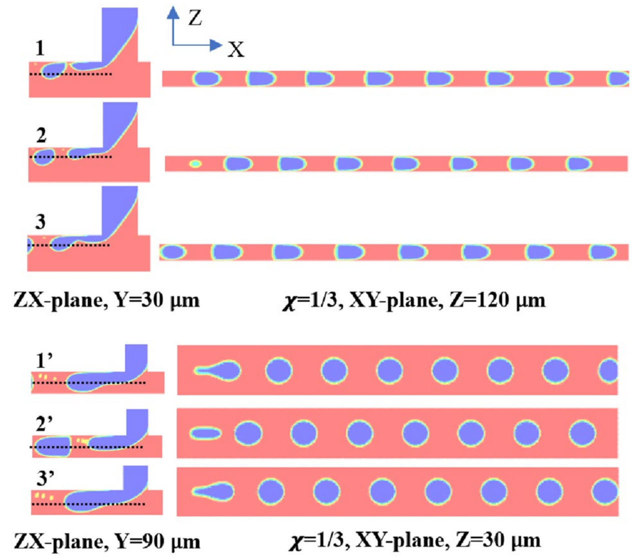

Fig. 9 The snapshots at the marked corresponding time

the stage II (2/2′ to 3/3′) due to the enlarging of void fraction of water droplets. The stage III is relative short (3/3′ to 4/4′), in which the droplet is pinched off the water stream and the pressure reduces suddenly. The stage III of both cases is about 0. 06 ms. There are some detailed differences at the curves of flow with the same capillary number but the reciprocal χ. Quantitatively, the stage I is slightly longer but the stage II is much shorter at the deep-style T-junction. It seems that there is a clear additional turning point between 1′ to 2′. It is marked as TP on the curve. The turning point is not clear on the curve of the flat-style T-junction because the generation of droplets is restricted beside the wall. It causes smaller perturbation to the mean flow. Overall, the droplets break up more quickly at the deep-style T-junction. The comparison here clearly shows that the difference is rooted from the shorter stage I plus stage II. The different style of confinement only takes effects on the former two stages. The stage III (pinching-off stage) is the same at both T-junctions because they break up according to the same Rayleigh–Plateau mechanism.

Figure 10 further shows the 3D generation dynamics of droplets at two paired T-junctions. The cross-sectional slices of the droplets inserted in the figure show that the shape of the droplets at two T-junctions is almost rotational symmetric at Ca = 0.01. There are no geometrical effects as the pressure (with isotropic feature) dominates the generation of droplets. At higher capillary numbers (Ca = 0.06), the size of droplets becomes smaller at the deep-style T-junction and they are positioned at the middle place of the channel. At both T-junctions, the droplets are generated at a tongue of water stream near the junction. The size of water tongues reduces and the body is elongated at Ca = 0.08, which results

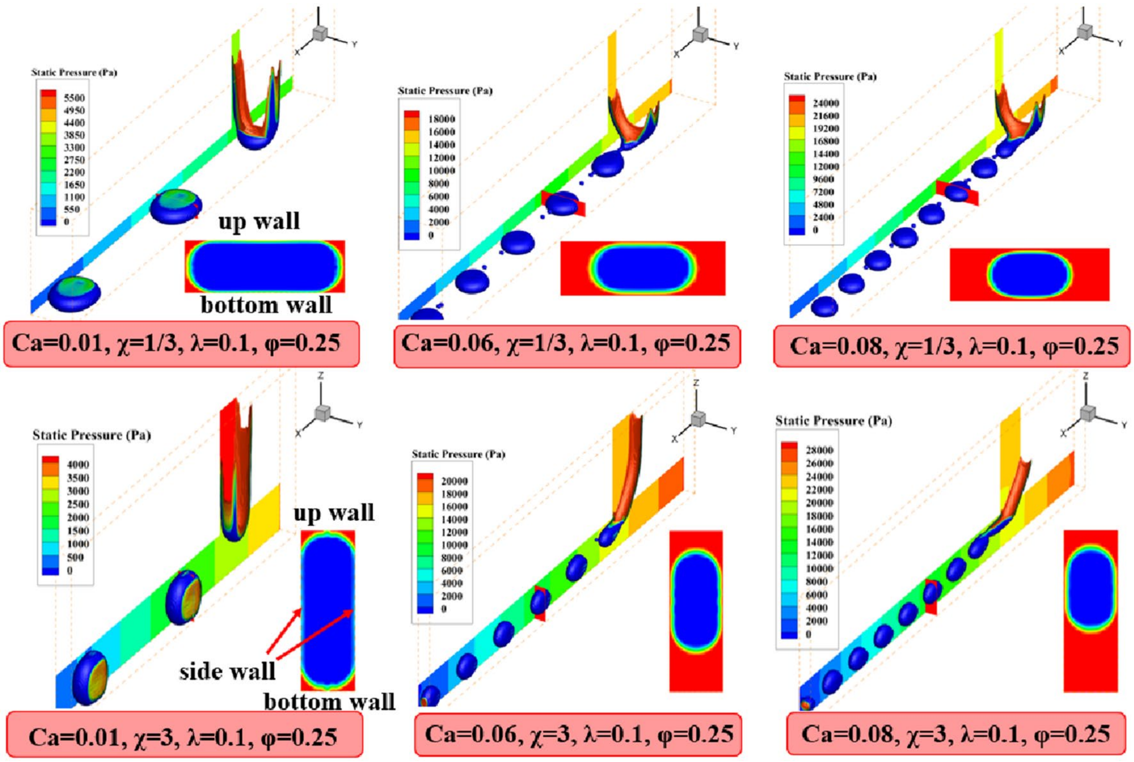

Fig. 10. 3D dynamics of droplet formation in two paired T-junctions ($\chi=3$ and $\chi=1/3$)

in a smaller perturbation to the continuous flow and thus a smaller variation of inlet pressure (shown in Fig. 8). It illustrates that the effects of pressure are attenuated at high Ca numbers at both T-junctions. In the two paired T-junctions, the flow rate and capillary number are the same. But the water stream contacts with the oil in different topological way in them, which leads to different degrees of confinement. It is observed that the tongue of water is finer and longer at the flat-style T-junction, compared to that of deep-style T-junction. It becomes more and more blunt as the χ reduces (not shown). It is interesting that the water stream becomes unbreakable in the studied domain if the χ is reduced to 1/10. Due to lack of enough shear strain rate at the directions of two side walls ($\chi = 1/10$), very long blunt tongues of water streams are generated (not shown), on which a throat is not formed at the domain with limit length and thus no droplets are generated. In this sense, a super-deep T-junction is equivalent to a 2-D T-junction. In a 2-D simulation of a T-junction with the same width of the channels and flow conditions, droplets are also not able to be generated (not shown).

van Stein et al. (2010) discussed the effects of geometrical confinement by comparing the breakup of water streams in confined and unconfined conditions. It was explained that the consequence of confinement is stable against small perturbations compared to similar problem found in unconfined geometries (Garstecki et al. 2005). In a classic Rayleigh–Plateau instability, the perturbations of the shape of the oil–water interface lead to rapid and irreversible collapse. The collapsing of the interface travels at the speed of a capillary wave. But in a confined condition, the progression of interface collapse is slow. The equilibration of the interfacial tension and hydrostatic pressure fields is faster, which results in uniform times of collapse of the thread and thus leads to uniform volumes of the produced droplets. Figure 11 shows the iso-surface of volume fraction of water (Ca$=$0.08, $\chi=3$ and $\chi=1/3$), flooded by shear strain rate. Figure 11b shows that the water stream (colored by blue) at the flat-style T-junction is positioned beside three walls of the channel. By comparison, it is mainly confined by the up and bottom walls at the deep-style T-junction (Fig. 11a). The different styles of confinement result in a blunt water tongue in the deep-style T-junction but a thin and elongated water tongue in the flat-style T-junction. Except these qualitative topological differences, the shear strain rate is different at two paired T-junctions in following aspects. The magnitude of strain rate at the throat of the breaking jet is higher in the deep-style T-junction. The distribution of high strain rate region locates near the throat, beside the up and bottom walls. Its distribution is non-uniform. Comparatively, it is seen that the strain rate in the flat-style T-junction is more uniformly distributed on the body of the water jet.

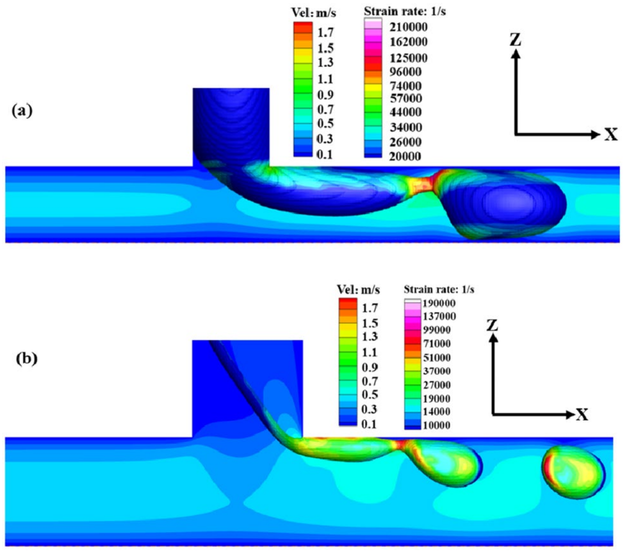

Fig. 11 The time history of throat of jets at the two paired T-junctions. **a** $\chi=1/3$, Ca = 0.08; **b** $\chi=3$, Ca = 0.08

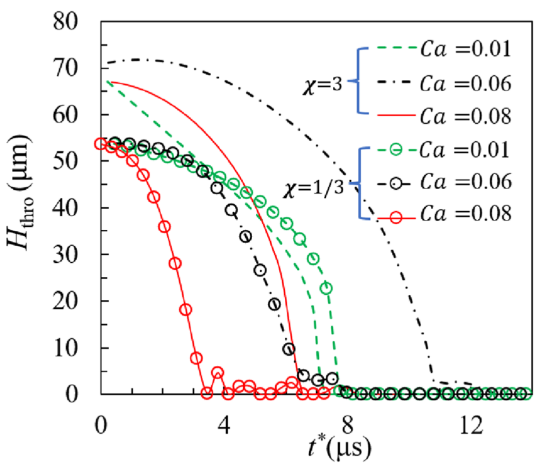

Fig. 12 Time history of the throat thickness of water streams at two paired T-junctions

The 3D observations here intuitively demonstrate that uniform strain rate induced by more confinement on the water stream leads to elongated jet and lower generation frequency. It agrees with the explanation of previous study (van Stein et al. 2010). The velocity contour in Fig. 11 further illustrates that the breakup position of the throat locates at the region of higher velocity gradient. It shows that at the deep-style T-junction, due to larger variation of velocity gradient, the strain rate at the throat becomes much higher as the jet is going to break up.

The time history of the throat (the width with fastest shrinking part) of water streams at the two paired T-junctions is plotted in Fig. 12. The scaled time (t^*) is the real time t (μs) multiplied by $Ca^{4/3}$. This treatment is to facilitate the comparison. The throat thickness is estimated from cross-sectional slices at Z–X plane. The sampling rate of the slices is 10,000 ftp. The variation patterns are similar except Ca = 0.01 and $\chi=3$, where the reduction of H_{thro} (dashed line) is linearly correlated to the t^* at the beginning. In other cases, it shows the law of exponential variation. The collapse time of the blunt water tongue is apparently shorter due to the higher strain rate imposed on it. Current study clearly illustrates that a 3-D tight confinement tends to stabilize the generation of droplets. This experience was already used in design of many devices, such as those flow-focusing microfluidic droplet generators (Yobas et al. 2006; Seo et al. 2007; Lashkaripour et al. 2019). In these devices, a channel with sudden reduced size was introduced to control the time scale of the stream of dispersed phase. However, before this study, the mechanism has not been studied in a clear and explicit way.

4 Conclusions and suggestions

In this paper, the generation dynamics of water–oil droplet flow at micro-T-junctions with various width-to-depth ratios are studied systematically via numerical method. Effects of width-to-depth ratios have been studied carefully, covering both flat-style T-junctions and deep-style T-junctions. Through comparing the droplet generation process at paired T-junctions with reciprocal width-to-depth ratios, some interesting effects of flow confinement are explicitly demonstrated. Following conclusions and suggestions are summarized:

1. The ratio of width-to-depth (χ) of a T-junction shows almost no effects on the generation of droplets as the capillary number of the continuous flow is less than 0.06. But at higher *Ca* numbers, the generation frequency increases and the droplet volume becomes smaller as χ reduces to less than 1/3. It is found that the power scaling law of droplet volume ($V_d \sim Ca^{-0.33}$) lasts for wider range of capillary numbers as the width-to-depth ratio of a T-junction is larger than 6. Varying the ratios of flow rates (0.1–0.4) and viscosity of two fluids (0.02–0.2) almost has no influence on the above scaling law as long as the flow is not stratified. It illustrates that at the same inlet conditions, the deep-style T-junctions generate droplets at higher frequency but lower pressure drops.
2. Although there are no geometrical effects of T-junctions as the droplets are generated at squeezing regime (pressure dominated), a 2-D T-junction still not able to produce the same result to that of a 3-D T-junction. In a 2-D T-junction, due to the lack of velocity perturbation in depth direction, the droplets are not able to be gener-

ated at a limit domain. It is shown that decreasing the width-to-depth ratio to the value less than 1/10 creates an equivalent 2-D effect in terms of droplets' generation. Without enough perturbation in depth direction, the droplets are not able to be generated at super-deep T-junctions.

3. The comparative study of the growth dynamics of a droplet in two paired T-junctions reveals that the topological structure of confinement has important effects on pinching-off stage of a droplet flow with high capillary numbers (Ca > 0.06). In a flat-style T-junction, the droplets are pinched off from a thinner and longer jet at high capillary numbers, which is confined to the side of three walls. The length of the jet becomes longer as the χ increases. Comparatively, in a deep-style T-junction, the droplets are pinched off from a thicker and blunt jet. The jet is mainly confined by two side walls. It is further found that the higher but more non-uniform strain rate is imposed on the tongues of the less confined jet at the deep-style T-junction. The less confined jet becomes more unstable at *Ca* higher than 0.06 because it locates at the region of higher velocity gradient, which leads to a much higher strain rate imposed on the throat of jets at the pinching-off stage. It compresses the pinching-off time, and thus the generation frequency of droplets in the deep-style T-junctions becomes higher.

Acknowledgements The project is supported by: (1) Guangdong Basic and Applied Basic Research Foundation, No. 2023A1515030105, 2022A1515140024; (2) Innovation Project of School of Education Department of China, No. 2020ZDZX2018; and (3) Guangdong Provincial Key Laboratory of Distributed Energy Systems, No. 2020B1212060075.

Author contributions KH—conceptualization, formal analysis, writing. ZZ—proof reading, data analysis. LZ—validation, video making. WZ—validation, plotting. SH—funding acquisition, supervision, reviewing.

Data availability The data that support the findings of this study are available within the article.

Declarations

Conflict of interest The authors have no conflicts to disclose.

References

Bai L, Fu T, Zhao S, Cheng Y (2016) Droplet formation in a microfluidic T-junction involving highly viscous fluid systems. Chem Sci Eng 145:141–148

Baroud CN, Gallaire F, Dangla R (2010) Dynamics of microfluidic droplets. Lab Chip 10:2032–2045

Basova EY, Foret F (2015) Droplet microfluidics in (bio) chemical analysis. Analyst 140:22–38

Bontoux N, Pepin A, Chen Y, Ajdari A, Stone HA (2006) Experimental characterization of hydrodynamic dispersion in shallow microchannels. Lab Chip 6:930–935

Brackbill J, Kothe DB, Zemach C (1992) A continuum method for modeling surface tension. J Comput Phys 100(2):335–354

Chakraborty I, Ricouvier J, Yazhgur P, Tabeling P, Leshansky AM (2019) Droplet generation at Hele-Shaw microfluidic T-junction. Phys Fluids 31:022010

Chen N, Wu J, Jiang H, Dong L (2011) CFD simulation of droplet formation in a wide-type microfluidic T-junction. J Dispers Sci Technol 33(11):1635–1641

Christopher GF, Anna SL (2007) Microfluidic methods for generating continuous droplet streams. J Phys D Appl Phys 40:R319

Christopher GF, Noharuddin NN, Taylor JA, Anna SL (2008) Experimental observations of the squeezing-to-dripping transition in T-shaped microfluidic junctions. Phys Rev E 78(3):036317

Cramer C, Fisher P, Windhab EJ (2004) Drop formation in a co-flowing ambient fluid. Chem Eng Sci 59(15):3045–3058

De Menech M, Garstecki P, Jousse F, Stone HA (2008) Transition from squeezing to dripping in a microfluidic T-shaped junction. J Fluid Mech 595:141–161

Feigl K, Tanner FX, Holzapfel S, Windhab EJ (2014) Effect of flow type, channel height, and viscosity on drop production from micro-pores. Chem Eng Sci 116:372–382

Garstecki P, Stone HA, Whitesides GM (2005) Mechanism for flow-rate controlled breakup in confined geometries: a route to monodisperse emulsions. Phys Rev Lett 94(16):194501

Garstecki P, Fuerstman MJ, Stone HA, Whitesides GM (2006) Formation of droplets and bubbles in a microfluidic T-junction-scaling and mechanism of break-up. Lab Chip 6(3):437–446

Glawdel T, Elbuken C, Ren CL (2012a) Droplet formation in microfluidic T-junction generators operating in the transitional regime II. Modeling. Phys Rev E 85(1):016323

Glawdel T, Elbuken C, Ren CL (2012b) Droplet formation in microfluidic T-junction generators operating in the transitional regime I. Experimental observations. Phys Rev E 85(1):016322

Gupta A, Kumar R (2010) Flow regime transition at high capillary numbers in a microfluidic T-junction: viscosity contrast and geometry effect. Phys Fluids 22(12):122001

Gupta A, Murshed SMS, Kumar R (2009) Droplet formation and stability of flows in a microfluidic T-junction. Appl Phys Lett 94(16):164107

Hatch AC, Patel A, Beer NR, Lee AP (2013) Passive droplet sorting using viscoelastic flow focusing. Lab Chip 13:1308–1315

He K, Lin Y, Hu Y, Huang SM (2022) Phase separation features of oil–water parallel flow at hydrophobic and hydrophilic micro-T-junction. Chem Eng Sci 253:117520

Hirt CW, Nichols BD (1981) Volume of fluid (VOF) method for the dynamics of free boundaries. J Comput Phys 39(1):201–225

Hoang DA, Portela LM, Kleijn CR, Kreutzer MT, van Steijn V (2013) Dynamics of droplet breakup in a T-junction. J Fluid Mech 717:R4

Hong YP, Wang F (2007) Flow rate effect on droplet control in a co-flowing microfluidic device. Microfluid Nanofluid 3:341–346

Husny J, Cooper-White J (2006) The effect of elasticity on drop creation in T-shaped microchannels. J Non-Newtonian Fluid Mech 30(1–3):121–136

Jena SK, Srivastava T, Bahga SS, Kondaraju S (2023) Effect of channel width on droplet generation inside T-junction microchannel. Phys Fluids 35:022107

Lashkaripour A, Rodriguez C, Ortiz L, Densmore D (2019) Performance tuning of microfluidic flow-focusing droplet generators. Lab Chip 19:1041–1053

Liu H, Zhang Y (2009) Droplet formation in a T-shaped microfluidic junction. J Appl Phys 106(3):034906

Liu ZM, Liu LK, Shen F (2015) Effects of geometric configuration on droplet generation in Y-junctions and anti-Y-junctions microchannels. Acta Mech Sinica 31:741–749
Loizou K, Wong V-L, Hewakandamby B (2018) Examining the effect of flow rate ratio on droplet generation and regime transition in a microfluidic T-junction at constant capillary numbers. Inventions 3(54):1–17
Mulligan MK, Rothstein JP (2012) Scale-up and control of droplet production in coupled microfluidic flow-focusing geometries. Microfluid Nanofluid 13:65–73
Nekouei M, Vanapalli SA (2017) Volume-of-fluid simulations in microfluidic T-junction devices: influence of viscosity ratio on drop. Phys Fluid 29:032007
Nisisako T, Torii T, Higuchi T (2002) Droplet formation in a microchannel network. Lab Chip 2:24–26
Pan D, Zhang Y, Zhang T, Li B (2021) Flow regimes of polymeric fluid droplet formation in a co-flowing microfluidic device. Colloid Interf Sci Commut 42:100392
Paramanantham SSS, Nagulapati VM, Lim H (2022) Numerical investigation of the influence of microchannel geometry on the droplet generation process. J Appl Fluid Mech 15(5):1291–1305
Rajesh VM, Buwa VV (2018) Volume-of-fluid simulations of gas-liquid-liquid flows in minichannels. Chem Eng J 345:688–705
Seo M, Paqyet C, Nie Z, Xu S, Kumacheva E (2007) Microfluidic consecutive flow-focusing droplet generators. Soft Matter 3:986–992
Soh GY, Yeoh GH, Timchenko V (2016) Numerical investigation on the velocity fields during droplet formation in a microfluidic T-junction. Chem Eng Sci 139:99–108
Sontti SG, Atta A (2017) CFD analysis of microfluidic droplet formation in non-Newtonian liquid. Chem Eng J 330:245–261
Thorsen T, Roberts R, Arnold F, Quake S (2001) Dynamic pattern formation in a vesicle-generating microfluidic device. Phys Rev Lett 86:4163–4166
Utada AS, Fernandez-Nieves A, Stone HA, Weitz DA (2007) Dripping to jetting transitions in coflowing liquid systems. Phy Rev Lett 99:094502
van Steijn V, Kleijn CR, Kreutzer MT (2010) Predictive model for the size of bubbles and droplets created in microfluidic T-junctions. Lab Chip 10:2513–2518
Wang X, Wang K, Riaud A, Wang X, Luo GS (2014) Experimental study of liquid/liquid second-dispersion process in constrictive microchannels. Chem Eng J 254:443–451
Wang S, Liu L, Wei S, Liu D (2019) Computational fluid dynamics simulation of water-oil two-phase slug flow in microchannels. Interf Phenom Heat Transf 7(4):365–376
Wehking J, Gabany M, Chew L, Kumar R (2014) Effects of viscosity, interfacial tension, and flow geometry on droplet formation in a microfluidic T-junction. Microfluid Nanofluid 16(13):441–453
White FM (1991) Viscous fluid flow, 2nd edn. McGraw-Hill, New York, pp 55–58
Wong VL, Loizou K, Lau PL, Graham RS, Hewakandamby BN (2017) Numerical studies of shear-thinning droplet formation in a microfluidic T-junction using two-phase level-SET method. Chem Eng Sci 174:157–173
Xu JH, Li SW, Tan J, Wang YJ, Luo GS (2006) Preparation of highly monodisperse droplet in a T-junction microfluidic device. Fluid Mech Transp Phenom 52(9):3005–3010
Xu JH, Tan J, Li S, Luo GS (2008a) Enhancement of mass transfer performance of liquid-liquid system by droplet flow in microchannels. Chem Eng J 141:242–249
Xu JH, Li SW, Tan J, Luo GS (2008b) Correlations of droplet formation in T-junction microfluidic devices: from squeezing to dripping. Microfluid Nanofluid 5(6):711–717
Xu L, Peng J, Yan M, Zhang D, Shen AQ (2016) Droplet synthesis of silver nanoparticles by a microfluidic device. Chem Eng Process Process Intensif 102:186–193
Yobas L, Martens S, Ong W-L, Ranganathan N (2006) High-performance flow-focusing geometry for spontaneous generation of monodispersed droplets. Lab Chip 6:1073–1079